

Point spread function measurement of an X-ray beam focused by a multilayer zone plate with narrow annular aperture

Hidekazu Takano,^{a*} Shigeki Konishi,^{a,b} Takahisa Koyama,^{a,c} Yoshiyuki Tsusaka,^a Satoshi Ichimaru,^d Tadayuki Ohchi,^d Hisataka Takenaka^{d,e} and Yasushi Kagoshima^a

^aCenter for Novel Material Science Under Multi-Extreme Conditions, Graduate School of Material Science, University of Hyogo, 3-2-1 Kouto, Kamigori, Ako, Hyogo 578-1297, Japan, ^bSpring-8 Service Co. Ltd, 1-20-5 Kouto, Shingu, Tatsuno, Hyogo 679-5165, Japan, ^cJapan Synchrotron Radiation Research Institute (JASRI/SPring-8), 1-1-1 Kouto, Sayo, Hyogo 679-5198, Japan, ^dNTT Advanced Technology Corporation, 3-1 Morinosato, Wakamiya, Atsugi, Kanagawa 243-0124, Japan, and ^eToyama Corporation, 4-13-16 Hibarigaoka, Zama, Kanagawa 252-0003, Japan. *E-mail: htakano@sci.u-hyogo.ac.jp

The experimental procedure for obtaining the point spread function (PSF) of a focusing beam generated using an X-ray multilayer zone plate (MZP) with a narrow annular aperture has been developed. It was possible to reconstruct the PSF by applying the tomographic process to the measured dataset consisting of line spread functions (LSFs) in every radial direction on the focal plane. The LSFs were measured by a knife-edge scanning method of detecting scattered intensity. In the experimental work, quasi-monochromatic undulator radiation with a first harmonic energy of 20 keV was directly focused without a monochromator by the MZP, and the PSF was measured using this procedure. As a result, a near diffraction-limited focused beam size of 46 nm full width at half-maximum was obtained.

Keywords: X-ray focusing; Fresnel zone plate; multilayer zone plate; point spread function; line spread function; computed tomography.

© 2014 International Union of Crystallography

1. Introduction

A Fresnel zone plate (FZP), the most standard X-ray focusing device, is a circular transmission grating with varied-zone spacing. The focusing size d depends on the narrowest and thus the outermost zone width Δr_N . A smaller fabricated Δr_N yields a smaller d . In the case of a circular aperture, d is defined as $1.22\Delta r_N$. Otherwise, the diffraction efficiency of the FZP depends on the thickness T in the X-ray propagating direction. Therefore, it is necessary to realise a high-aspect-ratio (T/d) zone structure for FZPs to be effective in the hard X-ray region. FZPs are conventionally fabricated by electron beam lithography (EBL). The EBL process is not suitable for fabricating zone structures with sufficiently high aspect ratios for hard X-ray use. A multilayer zone plate (MZP) was proposed by Rudolph *et al.* (1981) to realise a FZP with considerably higher aspect ratio zone structures and a much narrower outermost zone width than obtained by EBL. It can be fabricated by stacking multilayer pairs onto a cylindrical substrate, and by thinning the cross section to an effective thickness. A MZP for hard X-ray use was first demonstrated by Saitoh *et al.* (1989). A MZP with extremely high aspect ratio zones that can form the effective focus for 200 keV X-rays was demonstrated by Kamijo *et al.* (2009), and a MZP with very small Δr_N of 10 nm was also fabricated by Mayer *et al.* (2013). However, it is typically difficult for MZPs to achieve the diffraction-limited focusing size in comparison with FZPs fabricated by EBL because fabrication errors of zone structures during the multilayer stacking process are presently unavoidable and the errors seriously degrade the focusing

property. We have developed a relatively high precision MZP fabrication technique based on our previous development of linear focusing multilayer Laue lenses that can achieve a diffraction-limited line focus of 13.1 nm in FWHM (Koyama *et al.*, 2011). It is difficult to evaluate the focusing property of MZPs since they generally have a narrow annular aperture due to limitation of the multilayer stacking process. In the case of narrow annular aperture optics, a radial intensity profile of the point spread function (PSF) at the focal plane is highly different from that of the line spread function (LSF) that is usually obtainable from experimental results in the X-ray focusing evaluation. We have already reconstructed a PSF of the MZP by using a measured single LSF with the assumption that the MZP has an isotropic structure in the radial direction. The obtained PSF was in good agreement with Airy's pattern obtained from calculations using the diffraction integral (Koyama *et al.*, 2012). In this study, we obtained the actual PSF of the focused X-ray beam from a MZP by measuring LSFs in every radial direction in the focal plane and by using tomographic reconstruction (Herman, 2009).

2. Experiment

The experimental work has been performed at the synchrotron radiation beamline BL24XU (Tsusaka *et al.*, 2001) of SPring-8. Direct radiation from an X-ray undulator source with the first harmonic energy of 20 keV was used to prevent the incident X-ray wavefield from being disturbed by the beamline monochromator. A schematic

drawing of the experimental system constructed is shown in Fig. 1. The system was set up on an anti-vibration optical bench. An MZP (diameter: 62 μm ; outermost zone width: 40.4 nm; number of zones: 134; focal length for 20 keV X-rays: 40.5 mm) identical to one we previously reported (Koyama *et al.*, 2012) was used to form the focus to be measured. The annular aperture parameter ε (Born & Wolf, 1999) was 0.76, which gave a focusing size $d = 0.86\Delta r_N$. The other parameters and the fabrication are described elsewhere (Koyama *et al.*, 2012). A four-quadrant slit with an opening size of $\sim 3 \mu\text{m}$ in both vertical and horizontal directions was set $\sim 30 \text{ m}$ in front of the MZP in order to secure a sufficient spatially coherent area for incident X-rays illuminating the MZP. A platinum pinhole of diameter 20 μm was set near the focal plane. It was effective for extracting only the focusing beam of the first-order diffraction of the MZP. The measured intensity of the focused beam was $1.26 \times 10^8 \text{ photons s}^{-1}$. The focusing property was measured by a knife-edge scanning procedure in dark-field geometry (Suzuki *et al.*, 2005). A 300 μm -diameter platinum wire was used as the knife-edge. A lead sphere with a diameter of $\sim 1 \text{ mm}$ was set in front of the detector to configure the dark-field condition $\sim 170 \text{ mm}$ away from the focus. Then, the obstructive half-angle for scattered X-rays to the optical axis was 3 mrad in all radial directions. When the platinum wire was scanned across the focus in the focal plane, the intensity profile of the scattered X-rays was identical to a LSF, which is a line integral of the PSF in the parallel direction to the wire. A translation stage for the wire scanning was mounted on a rotation stage, the rotation axis of which was aligned almost identical to the optical axis. The measurement was performed as a two-dimensional scan in translation r and rotation θ as shown in Fig. 1. The scanning dimensions in r and θ were $5 \text{ nm} \times 1000$ points and $1.2^\circ \times 150$ projections with 0.2 s dwell time (step scan). In fact, there were large variations in the peak position (center position of focused beam) among the measured LSFs. The variations may be due to a physical and thermal drift of the positions between the focus and the rotation axes and by wobble in the rotational stage. The maximum variation of the intensity peak position during the entire r - θ scan was about 4.5 μm . The start position of each r scan was adjusted by using a peak position of the previous r scan in order to save the number of scanning points. Then, the measured LSFs were rearranged using each peak position to define the reconstruction center. The obtained LSFs in all radial directions are shown in Fig. 2. Unfortunately, in the last ten scans of the measured data the observed intensity became smaller. This is because of the misalignment between the MZP and the pinhole due to drift during the measurement. The obtained intensity distribution (Fig. 2) can be considered as a sinogram, which is used in tomographic reconstruction for a single cross section. The PSF thus reconstructed by a convolution back-projection algorithm (Ramachandran & Lakshminarayanan, 1971) is shown in Fig. 3(a). A concentric periodic pattern corresponding to Airy's pattern could be

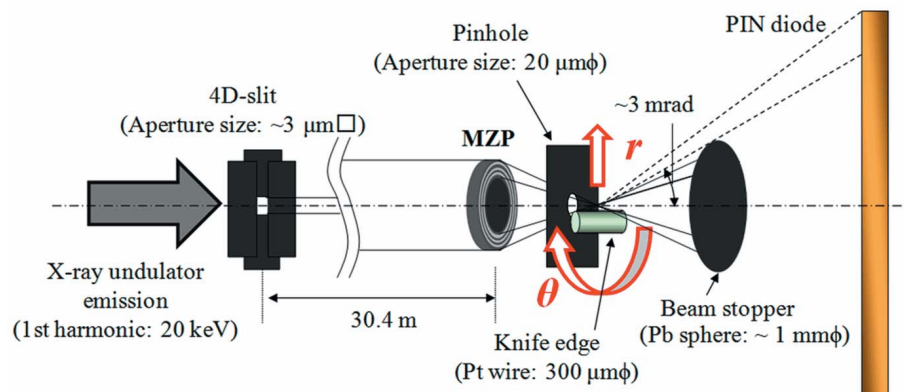


Figure 1
Optical system for evaluating PSF by the MZP.

obtained from this measurement. Fig. 3(b) shows a comparison between the averaged radial intensity profile and the ideal PSF calculated using the Fresnel–Kirchhoff integral with the designed zone structures. The focused spot size was thus evaluated to be 46 nm in FWHM, while the ideal size was 35 nm.

3. Discussion

In FZPs, the monochromaticity $E/\Delta E$ of the incident X-rays should be larger than the zone number of the FZP to avoid chromatic

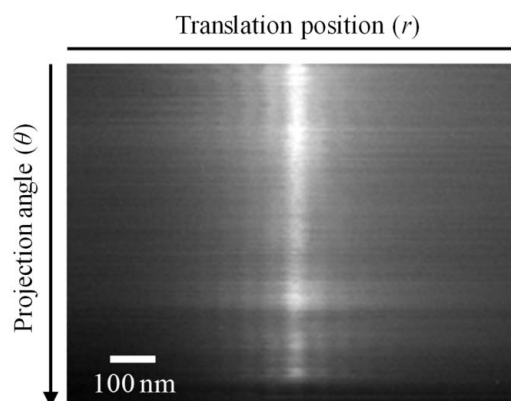


Figure 2
Measured LSFs with projection angles over 180° in the focal plane.

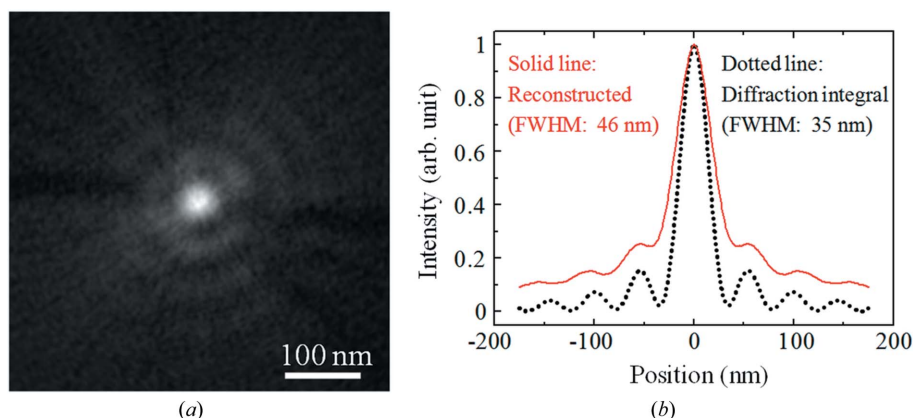


Figure 3
(a) Reconstructed PSF and (b) radial intensity profiles.

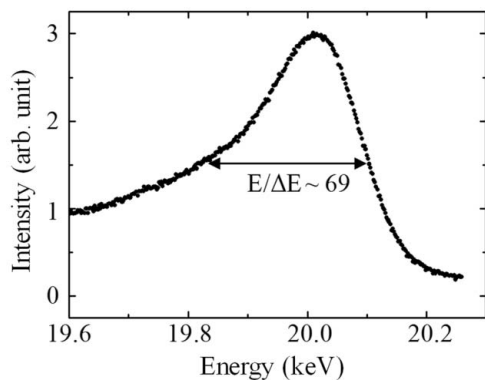


Figure 4
Spectrum of undulator emission measured using a beamline monochromator.

aberration. Fig. 4 shows the energy distribution of the incident X-rays measured by using a beamline monochromator (silicon double-crystal). The characteristic spectral distribution of the undulator harmonic emission could be obtained. A bandwidth of 69 ($E/\Delta E$ in FWHM) is smaller than the present number of zones, 134. Therefore, the incident monochromaticity seems insufficient from the theoretical point of view. Then, the focusing performance was investigated by calculations using the Fresnel–Kirchhoff integral. Fig. 5 shows the calculated PSF of the present MZP by considering the energy spread in Fig. 4. It can be concluded that the influence of the low monochromaticity on the focusing property is sufficiently small, although a slight influence could be observed for the outer side peaks. Moreover, the effective bandwidth might be smaller because the diffraction efficiency of the MZP for X-ray energies of over 20 keV becomes small owing to the K -absorption edge of Mo (20.00 keV) used as zone material of the MZP. There are some other reasons to be considered for the blurring of the experimentally obtained result. In the reconstruction procedure, errors in the correction process for the reconstruction center and the back-projection procedure [we used Chesler’s filter (Chesler & Riederer, 1975) in the back-projection] may be not negligible. However, the most serious effect may be caused by the fabrication errors in the MZP. Random errors in

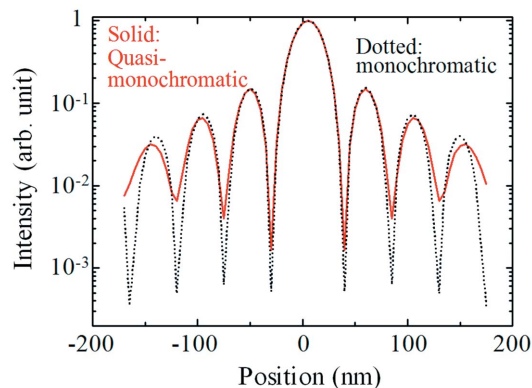


Figure 5
Calculated PSFs of the MZP for monochromatic X-rays (dotted line) and for X-rays with energy spread shown in Fig. 4 (solid line).

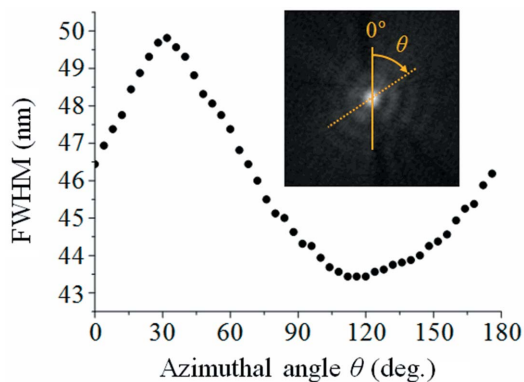


Figure 6
Azimuthal size distribution in the main peak reconstructed (in FWHM).

multilayer stacking may give isotropic blurring to the main peak; and deviation from circularity in the substrate may give anisotropy. In the result of the reconstructed PSF, the size of the main peak (in FWHM) was measured in every radial orientation as shown in Fig. 6. There may be no effect due to the failure in the measurement data between 168° and 180°, because the profile is smooth in the range. There is considerable azimuthal dependence with size between 43 nm and 50 nm. This astigmatism may be reflected in errors due to the substrate. However, it can be concluded that the PSF of an X-ray MZP having a narrow annular aperture can be measured by our proposed procedure using tomographic reconstruction and that the MZP achieves a near diffraction-limited focus.

This work was supported by SENTAN, Japan Science and Technology Agency (JST). The synchrotron radiation experiments were performed at BL24XU of SPring-8 with the approval of the Japan Synchrotron Radiation Research Institute (JASRI) (Proposal Nos. 2010A3200, 2010B3200, 2011A3200 and 2011B3200).

References

Born, M. & Wolf, E. (1999). *Principles of Optics*, 7th ed. (expanded), pp. 461–465. New York: Cambridge University Press.
 Chesler, D. A. & Riederer, S. J. (1975). *Phys. Med. Biol.* **20**, 632–636.
 Herman, G. T. (2009). *Fundamentals of Computerized Tomography*, 2nd ed. Berlin: Springer.
 Kamijo, N., Suzuki, Y., Takeuchi, A., Itou, M. & Tamura, S. (2009). *Jpn. J. Appl. Phys.* **48**, 010219.
 Koyama, T., Takano, H., Konishi, S., Tsuji, T., Takenaka, H., Ichimaru, S., Ohchi, T. & Kagoshima, Y. (2012). *Rev. Sci. Instrum.* **83**, 013705.
 Koyama, T., Takenaka, H., Ichimaru, S., Ohchi, T., Tsuji, T., Takano, H. & Kagoshima, Y. (2011). *AIP Conf. Proc.* **1365**, 24–27.
 Mayer, M., Keskinbora, K., Grévent, C., Szeghalmi, A., Knez, M., Weigand, M., Snigirev, A., Snigireva, I. & Schütz, G. (2013). *J. Synchrotron Rad.* **20**, 433–440.
 Ramachandran, G. N. & Lakshminarayanan, A. V. (1971). *Proc. Natl Acad. Sci.* **68**, 2236–2240.
 Rudolph, D., Niemann, B. & Schmahl, G. (1981). *Proc. SPIE*, **316**, 103–105.
 Saitoh, K., Inagawa, K., Kohra, K., Hayashi, C., Iida, A. & Kato, N. (1989). *Jpn. J. Appl. Phys.* **27**, L2131–L2133.
 Suzuki, Y., Takeuchi, A., Takano, H. & Takenaka, H. (2005). *Jpn. J. Appl. Phys.* **44**, 1994–1998.
 Tsusaka, Y., Yokoyama, K., Takeda, S., Takai, K., Kagoshima, Y. & Matsui, J. (2001). *Nucl. Instrum. Methods Phys. Res. A*, **467–468**, 670–673.